Received: 20 June 2023 | Revised: 22 November 2023 | Accepted: 3 December 2023

DOI: 10.1111/ijac.14675

International Journal of Applied Ceramic Technology

RESEARCH ARTICLE

Optimizing the structural and photocatalytic performance of Ag-decorated ZnO/Zn(OH)$_2$ nanoparticles for RhB degradation

Erman Erdogan[1] | **Cigdem Eden**[2] | **Nurtac Canpolat**[3] | **Cagri Cirak**[4] | **Mehmet Yilmaz**[5]

[1]Electronic Communication Technology Program, Vocational High School, Bilecik Seyh Edebali University, Bilecik, Turkey

[2]Department of Alternative Energy Sources, Vocational School, Erzincan Binali Yildirim University, Erzincan, Turkey

[3]Department of Chemistry, K.K. Education Faculty, Ataturk University, Erzurum, Turkey

[4]Department of Physics, Art & Science Faculty, Erzincan Binali Yildirim University, Erzincan, Turkey

[5]Department of Science Teaching, K.K. Education Faculty, Ataturk University, Erzurum, Turkey

Correspondence
Erman Erdogan, Electronic Communication Technology Program, Vocational High School, Bilecik Seyh Edebali University, 11100 Bilecik, Turkey.
Email: erman.erdogan@bilecik.edu.tr

Mehmet Yilmaz, Department of Science Teaching, K.K. Education Faculty, Ataturk University, 25240 Erzurum, Turkey.
Email: mehmetyilmaz@atauni.edu.tr

Abstract

In this study, as-prepared and Ag-decorated ZnO/Zn(OH)$_2$ composite nanoparticles (NPs) were obtained using the sol–gel technique. First, the effect of aging on the structural, optical, and morphological features was examined. Ag NPs can interact with the electronic structure of ZnO/Zn(OH)$_2$ NPs, resulting in changes in their energy levels. It was found that the composite NPs obtained after 6 h solution aging increased in full width at half maximum and good crystallinity of the structures from the X-ray diffraction (XRD) measurements. The Raman spectrum supports the experimental data obtained from XRD and Fourier transform infrared, a material containing a mixture of ZnO and Zn(OH)$_2$. From the morphological study, Ag NPs were successfully decorated on the ZnO/Zn(OH)$_2$ surface, and composite NPs did not change the morphological appearance of the structure. Second, the photocatalytic performance of the samples was investigated. In the experimental setting, ultra-violet A light was employed as the irradiation source, whereas rhodamine B (RhB) was used as the dyestuff. The photo-degradation of the RhB dyestuff on composite NPs was observed to be 98.5% and 92.5% for 6 and 2 h aged samples, respectively. On Ag NPs, the catalytic performance of the sample was increased up to 95% after 180 min.

KEYWORDS
photo-catalysis, RhB, traditional ceramics, Zn(OH)$_2$, ZnO

1 | INTRODUCTION

Nanotechnology has greatly contributed to the development of new materials by enabling the production of nano-sized particles with unique sizes and morphologies. Nanostructured metal oxide materials occupy an important place in many fields of chemistry, physics, materials science, and biotechnology.[1] Metal oxides form an attractive class of materials in the scientific world due to their interesting electrical properties ranging from insulator to semimetallic behavior, high dielectric constants, wide band gaps, and outstanding optical performance. In general, the d-shells of transition metal oxides are partially filled, whereas the shells of positive metal ions are filled with electrons. This unique electronic structure of metal oxides determines the material's metallic, semiconducting, or insulating properties.[2,3]

Thanks to its valuable properties in many places, ZnO has inevitably become one of the materials with applications in different fields. ZnO has an II–VI group, a large

E_g of 3.37 eV, and a significant binding energy of 60 eV at room temperature. The abundance of the element zinc and the low cost, non-toxicity, and chemical inertness of ZnO make it even more attractive.[4] Besides, its excellent transmittance, stability, and conductivity, especially at low substrate temperatures, make it a suitable candidate for various fields.[5] They have been used in areas, such as pH sensors, nanolasers, flexible devices, thin film transistors, transparent electrodes, spintronics, biosensors, optical memories, liquid-crystal displays (LCDs), touch panels, and organic light-emitting devices (OLEDs). ZnO also has good electronic and optical properties due to the non-stoichiometry caused by inherent defects such as oxygen vacancies and interstitial Zn atoms in the crystal lattice.[6] Depending on these properties, it generates electron-hole pairs under UV or visible light irradiation, making it suitable for different optical applications. For example, this generated electron-hole pair can interact with O_2 and H_2O adsorbed on the ZnO surface to form $\cdot O_2^-$ and $\cdot OH^-$, respectively, which can ultimately reduce and oxidize organic pollutants (such as dye) CO_2 and H_2O, respectively. This makes ZnO an alternative material for photocatalytic applications.

ZnO semiconductor photocatalyst has a large area in the removal of organic pollutants. In the photocatalytic oxidation process, ZnO interacts with ultra-violet A (UVA) as a source of radiation and converts to an active form. Studies have shown that ZnO is not only active in the visible range. In a study by Samad et al., ZnO's oxidation efficiency for the relief of As(III) in a single stage was combined with CuO, and a significant performance was achieved.[7] In another study, Hanh et al. made ZnO-added Cu synthesis to remove the MCP drug in the insecticide market. The synthesized Cu–ZnO photocatalytic performance was excellent, and they concluded that it increased the decomposition of MCP into CO_2, H_2O, and harmless substances.[8] Isai and his friends modified 2% of ZnO, preserving the hexagonal wurtzite structure. ZnO's photocatalytic efficiency increased, and the more promising activity of ZnO was produced.[9]

Many coating methods, such as sol–gel, hydrothermal, dip-coating, drop-casting, and successive ionic layer adsorption and reaction (SILAR) methods, have been used for coating ZnO structures.[10–12] Among these coating methods, the sol–gel method is preferred because of its versatility, low cost and low-temperature process, environmental compatibility, reusability, and durability. In addition, the sol–gel method offers good chemical and mechanical resistance, porous structure, homogeneous coating potential over a large area, and microstructure control.[13] The sol–gel method converts molecular precursors into an oxide network through hydrolysis and condensation reactions. Sol–gel chemistry involves hydrolysis to form reactive Zn–OH groups and condensation processes to form bridged oxygen.[14]

He et al. investigated the performance of ZnO nanostructures prepared by the precipitation–calcination method in methylene blue dye and observed a maximum performance of 92%.[15] Zhang et al. also reported the photocatalytic activity of vacuum-assisted ZnO nanoparticles (NPs) in methylene blue dye with high performance.[16] In another study, ZnO thin films deposited by a high vacuum technique showed high photocatalytic performance for orange G dye in the liquid phase.[17] Compared to the methods mentioned above that require vacuum, which is difficult, complex, and costly, the ZnO structures that we have obtained relatively easily in our study have provided an alternative to the literature mentioned above by using them in photocatalytic applications with similar or higher performance.

Our research investigated the synthesis and characterization of hybrid ZnO/$Zn(OH)_2$ structures. This area has yet to be thoroughly explored compared to the extensive research on pure and doped ZnO NPs. This particular hybrid configuration has demonstrated the ability to create synergistic effects that significantly improve photocatalytic performance. This can be attributed to the dye molecules, which can form intermolecular and intramolecular bonds due to the presence of a large number of hydroxyl groups. In addition, silver NPs (Ag NPs) were deposited on the surface of this hybrid structure to enhance the catalyst's photocatalytic activity of the catalyst by acting as an electron trap to prevent electron–hole recombination. This study's results may guide future research aimed at optimizing photocatalytic efficiency. The information presented here will broaden the scope of hybrid nanomaterials while paving the way for the investigation of comparable hybrid structures containing diverse material combinations. In this research, the X-ray diffraction (XRD), Fourier transform infrared (FTIR) spectroscopy, Raman spectroscopy, UV–vis spectrophotometer, scanning electron microscopy (SEM), and energy-dispersive X-ray (EDX) measurements were used to examine the optical properties, surface morphologies, and structural characteristics of as-prepared and Ag-decorated ZnO/$Zn(OH)_2$ NPs.

2 | EXPERIMENTAL PROCEDURES

In the synthesis of ZnO nanostructures, zinc acetate dihydrate ($C_4H_{10}O_6Zn$) was employed as our zinc precursor, identified by its CAS number 5970-45-6, obtained from Carlo Erba. NaOH pellets with CAS number 1310-73-2 were used to adjust the pH of the prepared precursor solutions. In the initial step of the experimental procedure, approximately 2.31 g of $C_4H_{10}O_6Zn$ were dissolved

in 100 mL of deionized water at room temperature. This solution was stirred for approximately 30 min at the same temperature to achieve a more uniform mixture. Some prior research has shown that the morphology of ZnO nanostructures derived from the zinc acetate precursor varies with pH. Specifically, ZnO nanostructures exhibited a rodlike morphology when the pH of the Zn precursor solution at 11 and 13.[18] Therefore, the pH of the solution was adjusted to 11. The pH 11 solutions were stirred on a magnetic stirrer at 80°C for 2 h and then cooled to room temperature. The resulting precipitate underwent washing with deionized water and ethanol and was subsequently dried in an oven at 80°C for 6 and 2 h. Finally, we decorated the $ZnO/Zn(OH)_2$ composite nanostructures, which had undergone a 2-h drying process, with Ag NPs prepared using the oleic acid and oleylamine reduction method developed by our research team, as described in the literature to enhance their photocatalytic performance.[19] Multiple techniques were employed to analyze the prepared samples. XRD was conducted using a PANalytical Empyrean diffractometer equipped with Ni-filtered CuK_α radiation (the instrument was operated at 45 kV and 40 mA at room temperature to produce X-rays with a wavelength of $\lambda = 1.54\,050$ Å). Raman was performed using a WITech Alpha 300R micro-Raman spectrometer with a back-illuminated CCD detector. In addition, the surface morphology and optical properties of the samples were evaluated using Quanta FEG 450-FEI brand SEM, Shimadzu UV-3600 Plus UV–vis–NIR spectrophotometer, and Thermo Nicolet 6700 brand FTIR spectroscopy at 4 cm^{-1} resolutions, respectively. The photocatalytic performances of the obtained $ZnO/Zn(OH)_2$ nanostructures were investigated by the photo-degradation of rhodamine B (RhB) dye. $ZnO/Zn(OH)_2$ nanostructures were adjusted to a concentration of .1 g/L, transferred to a cuvette filled with 5 mL of aqueous RhB solution (5 ppm), and kept in the dark for 30 min. A photo-reactor apparatus (Luzchem, LZC-4X) comprising a UVA lamp, emitting a wavelength of 350 nm with a power density of 1000 W/m^2, was utilized as the light source.

For photo-catalysis studies, the UVA source and the sample were also placed at a distance of 10 cm. A UV–vis spectrophotometer (PG Instruments, T80+) was used to study the photo-degradation of RhB, and residual concentrations of RhB at 554 nm were obtained at determined times according to the Beer–Lambert law. As stated previously, determining C/C_0 values, which indicate the RhB concentration over time, is crucial for investigating photo-catalysis procedures. C signifies the concentration of RhB at a specific time during the experiment and was obtained via measurement of the sample's absorbance at a specified wavelength. The C_0 term denotes the initial RhB concentration in the reaction mixture. It is typically determined by evaluating the initial absorbance or the known concentration of the RhB solution before the photo-catalysis experiment. Therefore, the RhB solution prepared at a concentration of 5 ppm was kept in the dark for 30 min before the catalyst was added, and the C/C_0 curves obtained under these conditions were analyzed for photo-catalysis performances.

3 | RESULTS AND DISCUSSIONS

3.1 | XRD investigations

The XRD spectra of the two composite NPs (6 and 2 h aged) produced due to solution aging are given in Figure 1A,B. The most dominant peak of the ZnO structure is in the orientation (101) with an angle of 2θ of around 36°. The XRD patterns show that the crystal structure of the 6 and 2 h structures is hexagonal, according to PDF card no. 36-1451. From the XRD results, it was seen that the coated 6-h-aged structure had a crystal structure. In addition, the $Zn(OH)_2$ peaks, including a little bit of water with the PDF card no. 20-1436, decreased, and sharper and higher intensity peaks appeared in the sample, which was grown after 6 h of aging, compared to the sample grown after 2 h of aging, which shows us that the ZnO structure has emerged. Parameters such as the crystal structure of the produced composite NPs and the calculated crystallite size are related to the intensity of the peaks and the half maximum width (FWHM) values.[20] Crystallite sizes are inversely proportional to the FWHM value of the diffraction peak obtained by XRD. The fact that the diffraction peak is relatively narrow and sharp corresponds to a large crystallite size and good crystallization. As seen in the figures, the peak intensities of the composite NPs, which were grown as the solution aged, increased, and narrow and sharp peaks were formed.

The XRD pattern of the Ag-decorated ZnO structure is shown in Figure 1C. The polycrystalline nature of the Ag-decorated ZnO structures is visible from the XRD pattern. All peaks were indexed, and Ag-decorated ZnO was compatible with that of the hexagonal phase. As the significant 2θ values of both materials are very close, the value of 2θ, a severe peak, was observed in the spectrum. The peak position or intensity of Ag NPs is cubic according to PDF card no. 04-0783. It is seen that it is pretty compatible with the Ag@ZnO NPs or nanostructures obtained in the literature.[21] Sakir et al. reported that the crystallite size for ZnO was around 57.6 nm, and for AuNPs@ZnO, it was around 21 nm in their study.[22]

To analyze the growth of crystals, the particle size (D) of samples was calculated by measuring the width

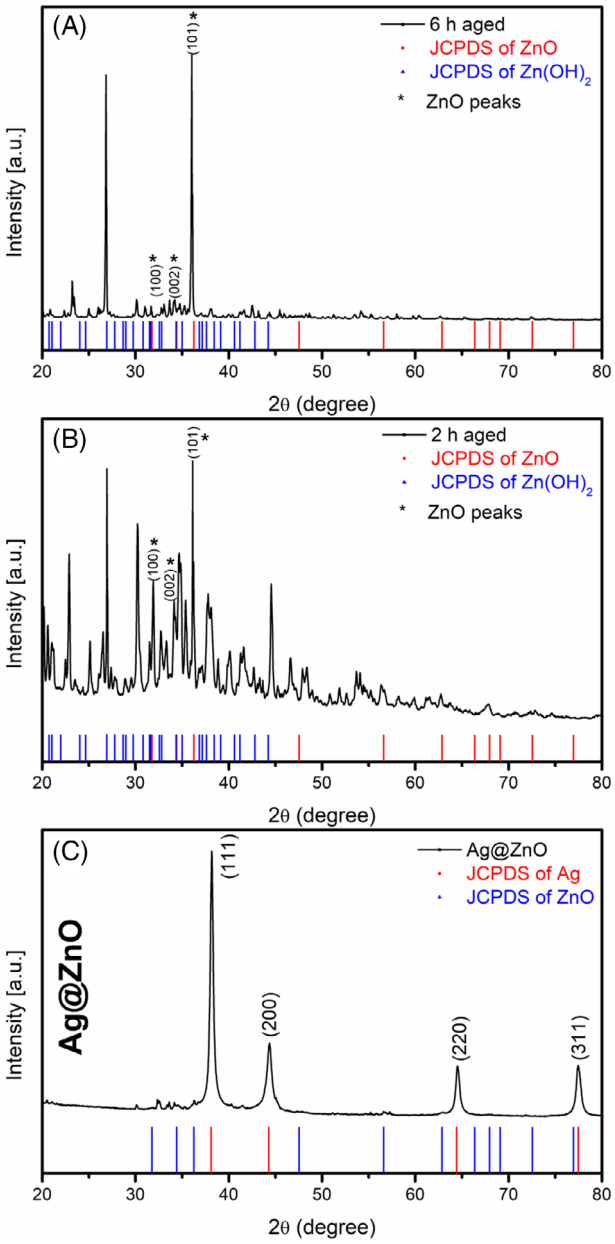

FIGURE 1 X-ray diffraction pattern of samples after (A) 6 h, (B) 2 h aging times, and (C) Ag@ZnO.

corresponding to half the height of the diffraction peaks using the following modified Scherrer equation[23]:

$$\ln\beta = \ln\frac{0.9\,\lambda}{D} + \ln\frac{1}{\cos\theta}$$

where D is the size of the crystal, λ is the incident X-ray wavelength (1542 Å), β is the FWHM, and θ is the angle of the XRD peaks. As can be seen from Figure 2A,B, if we plot the data for lnβ to ln (1/cosθ), a slope with a line and a crossing of ln $0.9\lambda/D$ should have existed. By using this equation, the crystal sizes were found in decreasing order and are given in Table 1.

In the Williamson–Hall (W–H) method, sinθ is used instead of 1/cosθ as in the Scherrer equation. This important fundamental difference allows for the separation of microstructural, small crystalline size, and a reflection enlarged by micro tension. Accordingly, the crystal dimensions can be calculated by the following equation[24]:

$$\beta\cos\theta = \frac{K\lambda}{D} + 4\varepsilon\sin\theta$$

where β is the full width at the middle maximum at 2θ, θ is the diffraction angle, K is a constant equal to 0.9, λ is the X-ray wavelength (0.154 nm), D is the crystal size in nm, and ε is the lattice tension. Figure 3A,B shows the graphs of different aging time-coated ZnO structures by the W–H method and Ag-decorated ZnO structure, respectively. The crystallite size found by the Scherer equation shows a significant decrease with increasing aging time compared to the results obtained from the W–H method. The main reason for the variability here is that the internal stresses are not included in calculating the crystallite size in the Scherrer method.[25]

3.2 | Optical investigations

Diffuse reflectance spectroscopy can be easily applied to solid-powder samples from the UV to IR regions. This method calculates the band gap energy of semiconductors by collecting the light resulting from the absorption and scattering of the material and converting it into quantitative data.[26] UV–vis diffuse reflectance spectra of ZnO/$Zn(OH)_2$ structures at different aging times and Ag-decorated ZnO are given in parts (a) and (b) of Figure 4, respectively.

The data obtained by this technique are used to calculate the band gaps of semiconductors using the following Kubelka–Munk function[27]:

$$F\,(R) = \frac{(1-R)^2}{2R} = \frac{K}{S}$$

where R is the diffuse reflectance of the sample, and K and S represent the absorption and scattering coefficients. The band gap energy (E_g) of the semiconductor sample can be determined by linear plotting of $[F(R)h\upsilon]^2$ versus $h\upsilon$. The optical band gap values of the obtained structures as a result of the aging of 2 and 6 h were found to be 3.59 and 2.89 eV for ZnO phase and 5.32 and 5.20 eV for $Zn(OH)_2$ phase, respectively. Band gap values of different solution-aged samples in the UV–vis diffuse reflectance spectra of ZnO/$Zn(OH)_2$ composite NPs in Figure 5A are corresponded to $Zn(OH)_2$ phase, which is in good agreement in the literature.[28] As the solution aged, the

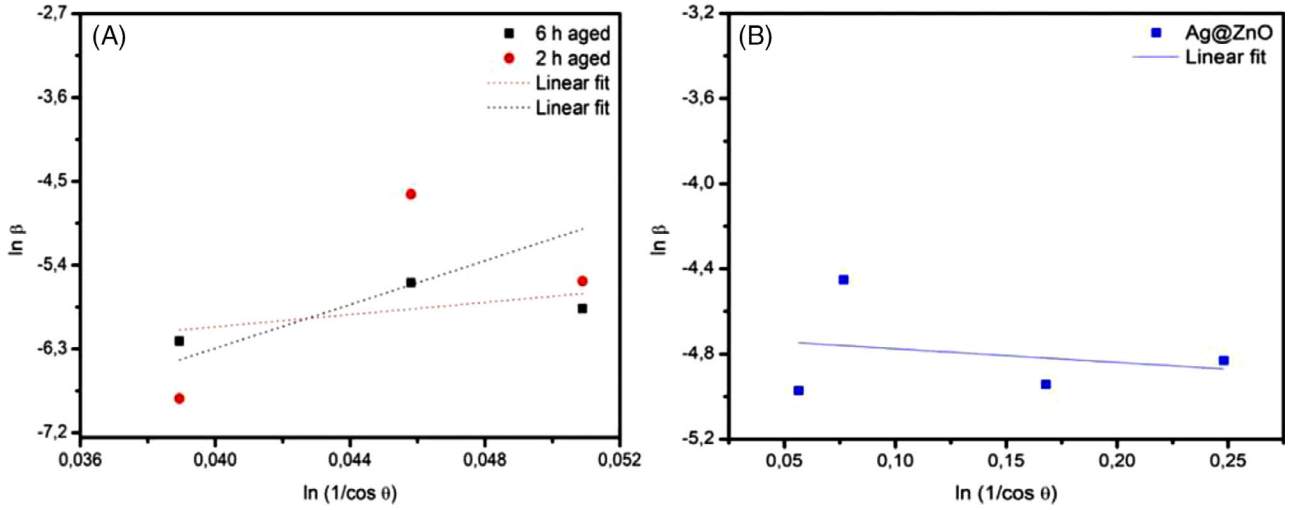

FIGURE 2 Graphs of (A) 6 and 2 h aging times and (B) Ag@ZnO samples by the modified Scherrer method.

TABLE 1 Various parameters from structural examination.

Aging time	(*hkl*)	d_{hkl} (Å)	2θ (°)	FWHM (°)	D_{SR} (nm)	D_{WH} (nm)
6 h	(100)	2.8279	31.60	.1145	52.34	115.50
	(002)	2.6075	34.35	.2143		
	(101)	2.4771	36.85	.1624		
2 h	(100)	2.8132	31.77	.2184	60.37	116.00
	(002)	2.6024	34.42	.5546		
	(101)	2.4751	36.25	.0619		
Ag@ZnO	(111)	2.3555	38.16	.3968	15.41	12.48
	(200)	2.0413	44.32	.6684		
	(220)	1.4415	64.57	.4084		
	(311)	1.2311	77.43	.4572		

Note: d_{hkl}, interplanar distance; D_{SR}, the size of crystal obtained from Scherrer plot; D_{WH}, the size of crystal obtained from Williamson–Hall plot.
Abbreviations: FWHM, full width at half maximum.

band gap of the samples decreased. Changes in optical band gaps relative to ZnO nanostructure morphology further confirm that nanostructure crystallinity, crystal growth directions, intrinsic defects like oxygen vacancies, and crystal grain size lead to a smaller effective band gap of nanostructured ZnO than the bulk value of 3.37 eV.[29] In addition, a decrease in the band gap of both ZnO and $Zn(OH)_2$ phased was observed with the addition of Ag NPs on the surface of the $ZnO/Zn(OH)_2$ structure. The possible reasons for this situation are discussed as follows. Ag NPs exhibit surface plasmon resonance (SPR), a phenomenon that occurs when the conduction electrons in the NPs are collectively released in response to incident light. The absorption of photons at specific wavelengths by Ag NPs can change the overall optical properties of the composite. The SPR of Ag NPs can interact with the electronic structure of $ZnO/Zn(OH)_2$ NPs, resulting in changes in their energy levels. This interaction can effectively reduce the band gap of the composite, making it more sensitive to lower energy photons. In addition, the presence of Ag NPs on the surface of $ZnO/Zn(OH)_2$ NPs can introduce defects and surface states into the composite material. These defects and surface states can trap charge carriers (electrons and holes) and create localized energy levels in the band gap. This can lead to a reduction in the effective band gap observed in the material. As a result, the interaction between Ag and the $ZnO/Zn(OH)_2$ surface can also lead to changes in the energy levels of the semiconductor, affecting its optical properties. Similar observations have been made by the other researcher for Ag-decorated ZnO.[30,31] The colloid structure of the solution being more stable due to aging and the formation of a longer compound network allowed the produced composite NPs to become more stable.

It is seen that the band gap values calculated for the Ag-decorated ZnO, as seen in Figure 5B, are very close to the sample aged for 6 h. This already shows us that the Ag-decorated ZnO nanostructure was made from a sample aged for 6 h. We see similar studies in the literature, which show very close band gap values of ZnO

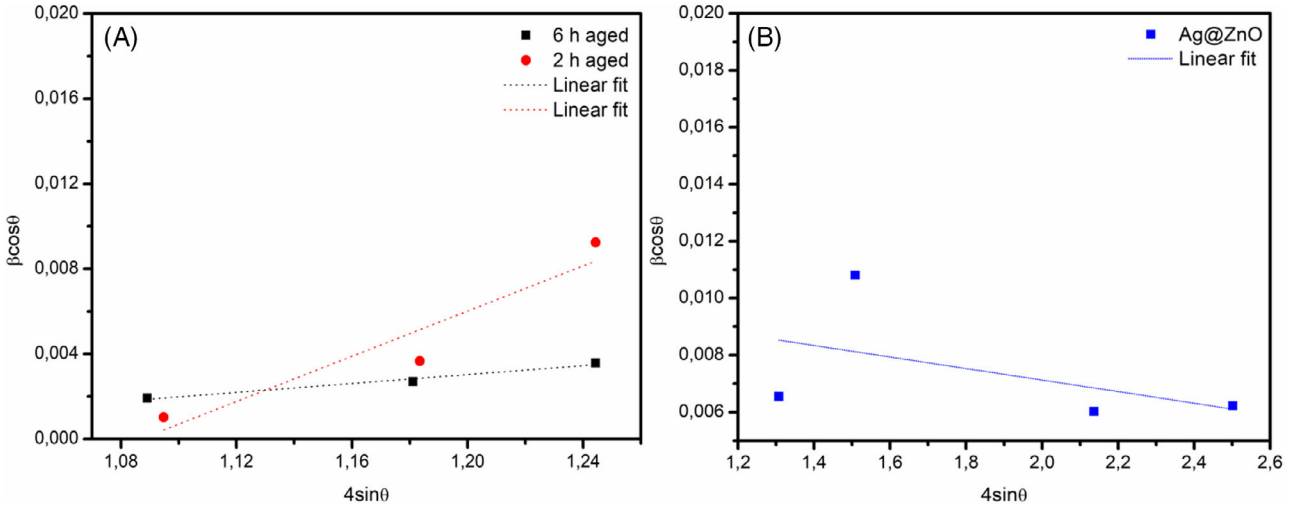

FIGURE 3 Graphs of (A) 6 and 2 h aging times and (B) Ag@ZnO samples by the Williamson–Hall (W–H) method.

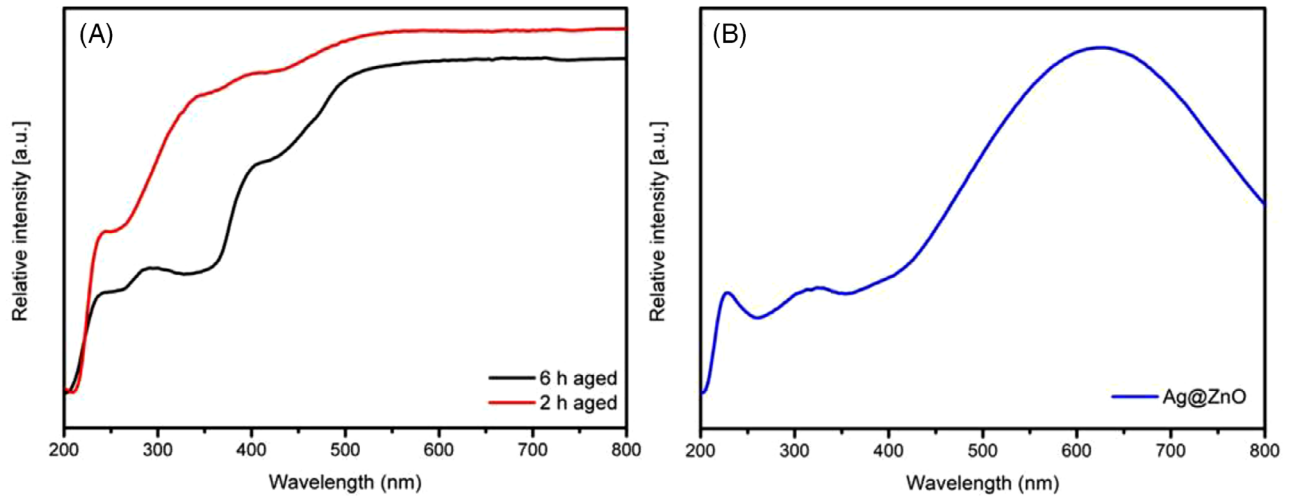

FIGURE 4 UV–vis diffuse reflectance spectra of (A) ZnO/$Zn(OH)_2$ structures with various aging times and (B) Ag-decorated ZnO.

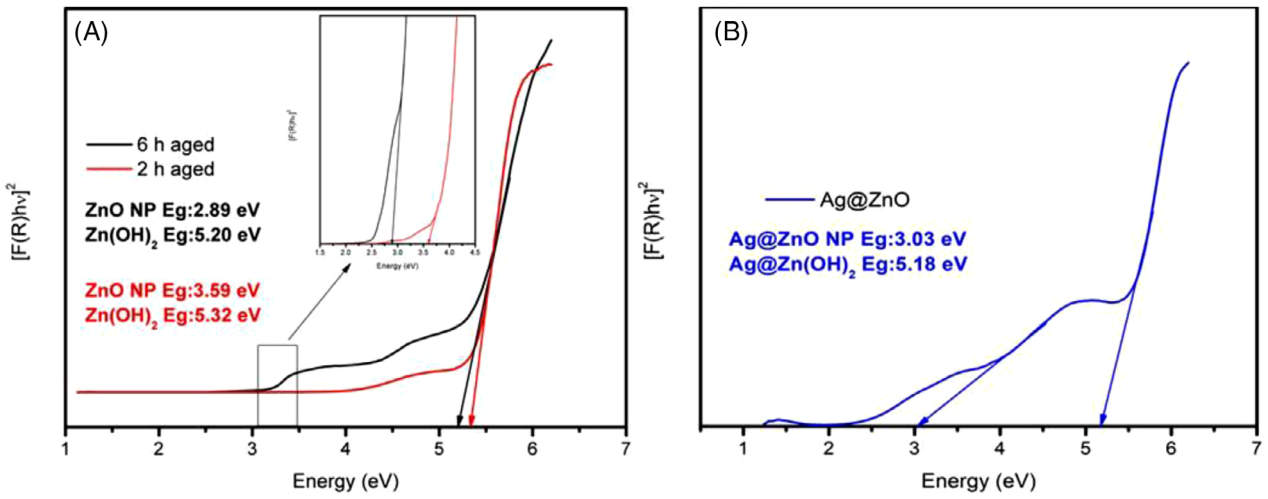

FIGURE 5 Kubelka–Munk graph of samples after (A) 6 and 2 h aging times and (B) Ag@ZnO.

and Ag/ZnO nanostructures.[32] This shows us that the nanostructure we obtained was successfully synthesized with Ag decoration.

3.3 | Morphological investigations

SEM images were taken to examine the surface morphology and nanostructure of the obtained samples after different aging times. From the SEM images (see Figure 6), it is seen that the surface morphology is affected by the aging time. The imaged composite NPs give the appearance of a granular structure composed of tiny grains that appear to be aggregated with some porosity. As the aging time increased, we saw that the composite NPs were denser structures made up of larger particles characterized by more effectively packed nanocrystals. Ag NPs were successfully decorated on the ZnO surface, and both Ag and ZnO NPs did not change the morphological appearance of the structure. Ag-decorated SEM image clearly shows that it was found that Ag NPs were seen as bright particles. Results from SEM images are consistent with observations from XRD.

EDX spectroscopy analysis was performed to determine the chemical compositions and mineralogical structures of Ag-decorated ZnO and ZnO with different aging times (see Figure 7). The characteristic Zn, O, and C elements were determined in the EDX analysis of the samples obtained after 6 and 2 h of aging. Except for these peaks, no severe and characteristic peaks were observed. In the EDX analysis of Ag-decorated ZnO, ZnO characteristic elements and Ag elements were determined. In particular, the presence of the Ag element shows that the nanostructures in ZnO are not replaced by Ag ions; they do not enter between the layers and are only decorated on the surface of the ZnO structure.

3.4 | FTIR investigations

To qualitatively determine the composition and possible interaction of the components of the samples and their chemical content and to determine the functional groups of ZnO, $Zn(OH)_2$, and Ag-decorated ZnO for different aging times, FTIR analysis was performed, and the obtained spectra are given in Figure 8A,B. Due to their interatomic vibrations, metal oxides generally give an absorption band below 1000 cm^{-1} wave number. In the literature, the absorption peak of 453 cm^{-1} wave number corresponds to the Zn–O stretch band in the ZnO lattice. It has been reported as a characteristic peak representing the ZnO structure.[33] In our study, the absorption peak at wave numbers 635 and 488 cm^{-1} indicates the Zn–O

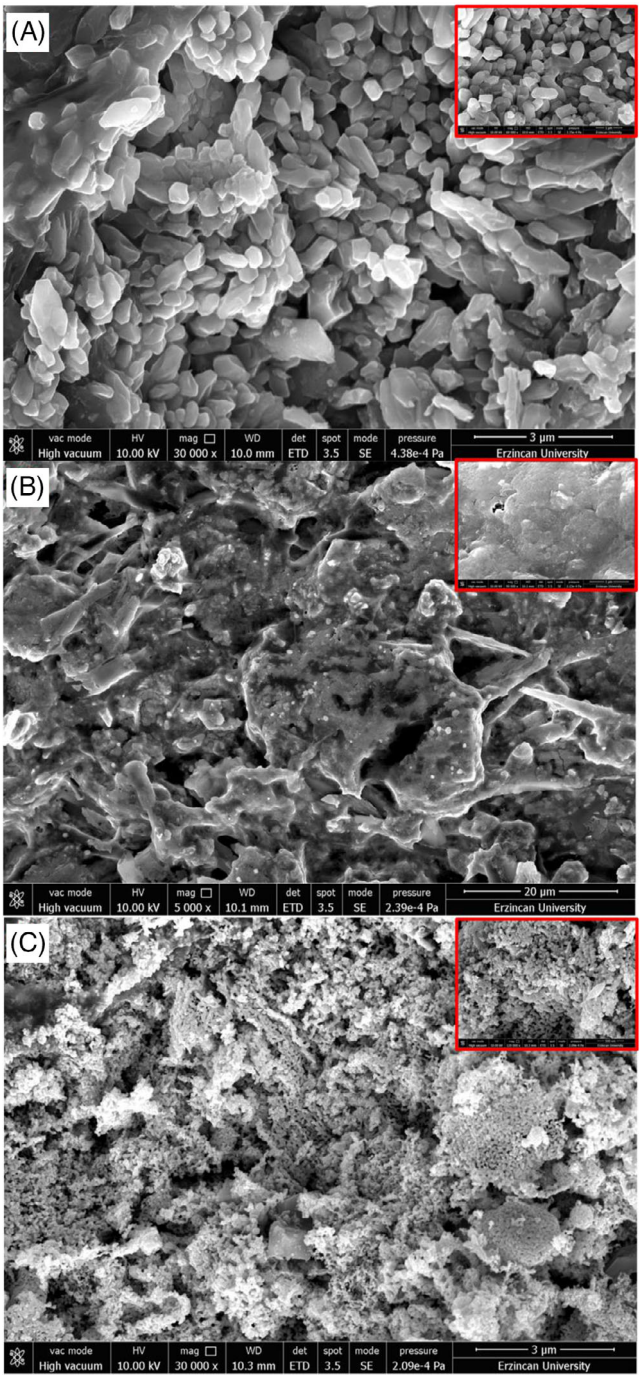

FIGURE 6 Scanning electron microscopy (SEM) images of the ZnO for (A) 6 h aging time, (B) 2 h aging time, and (C) Ag@ZnO sample. (The inset surrounded by red shows the magnified surface morphology.)

stretch in the ZnO lattice. Peaks at a wave number value of 1000 cm^{-1} correspond to the characteristic bands of $Zn(OH)_2$.[34] In our study, these peaks correspond to 877, 919, and 1002 cm^{-1} wave numbers. The bands at 2923 and 2996 cm^{-1} can be attributed to the symmetric–asymmetric C–H stretching vibration. The bands between 1400 and 1600 cm^{-1} are related to the C = O stretching vibration

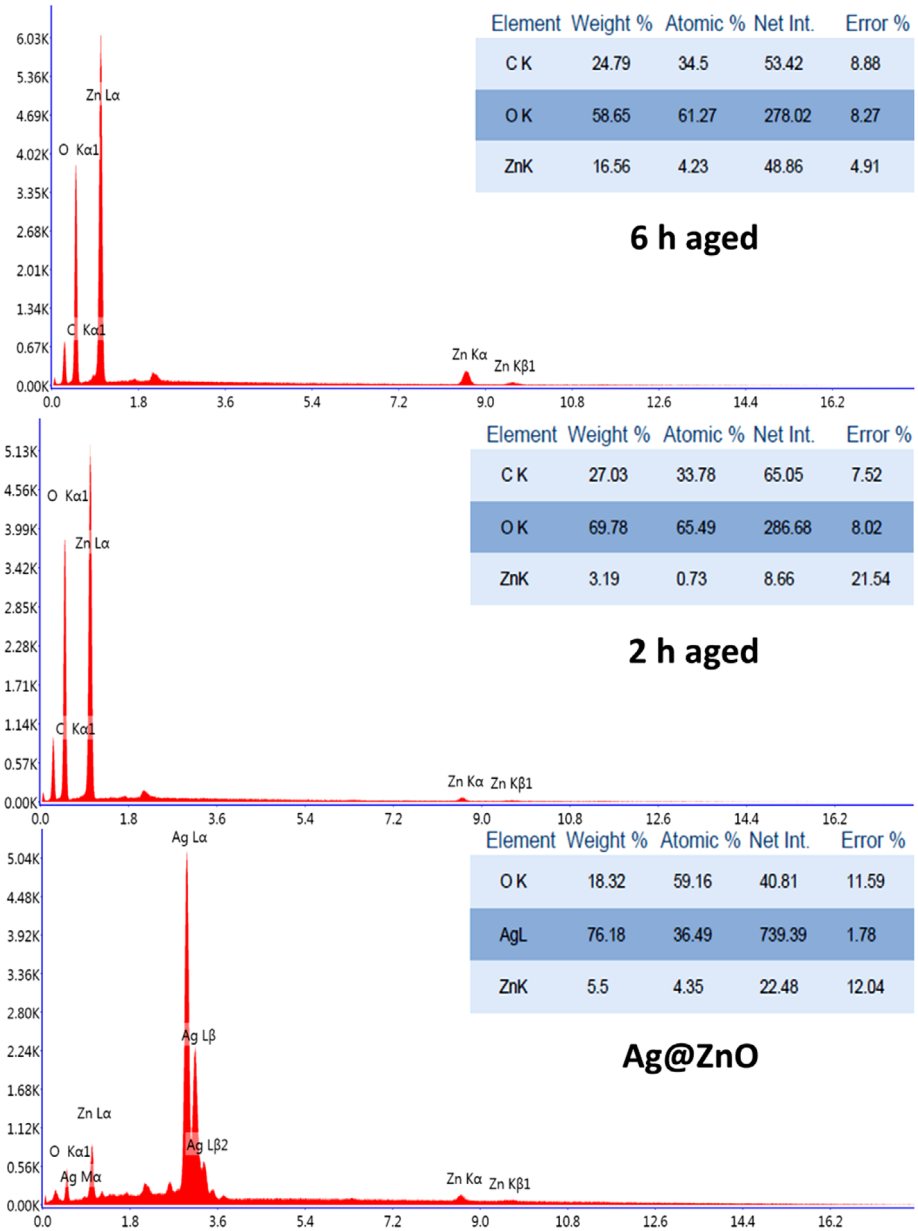

FIGURE 7 Energy-dispersive X-ray (EDX) spectrum of synthesized ZnO samples with different aging times and Ag@ZnO sample.

of ZnO and Ag-decorated ZnO structures. The peak band observed at the wave number value of 3600 cm^{-1} is due to the O–H bonds belonging to the small amount of water remaining on the surface of the crystals.[35]

The lack of displacement of the IR bands of ZnO and the absence of new IR bands show that Ag NPs are decorated on the structure surface, and related spaces without bonding with ZnO, and these data are also supported by other techniques. Few Ag ions can be demoted to Ag^0 by hydroxyl groups from the ZnO and $Zn(OH)_2$ structures. If this oxidation takes place, band formation to the carbonyl group (C = O) will appear at 1634 cm^{-1}.[36,37]

3.5 | Raman investigations

Raman spectroscopy is a vibration spectroscopy with a wide application area in the academic field. With this method, information can be obtained about the bonds made by the atoms or molecules that make up matter by examining the inelastic scattering of photons sent from the light source by the atoms or molecules.[38] Raman spectrum was obtained on a micro-Raman spectrometer equipped with a DPSS laser emitting at 532 nm wavelength. The laser power on the sample was kept at 10 mW to avoid laser-induced sample annealing and modification.

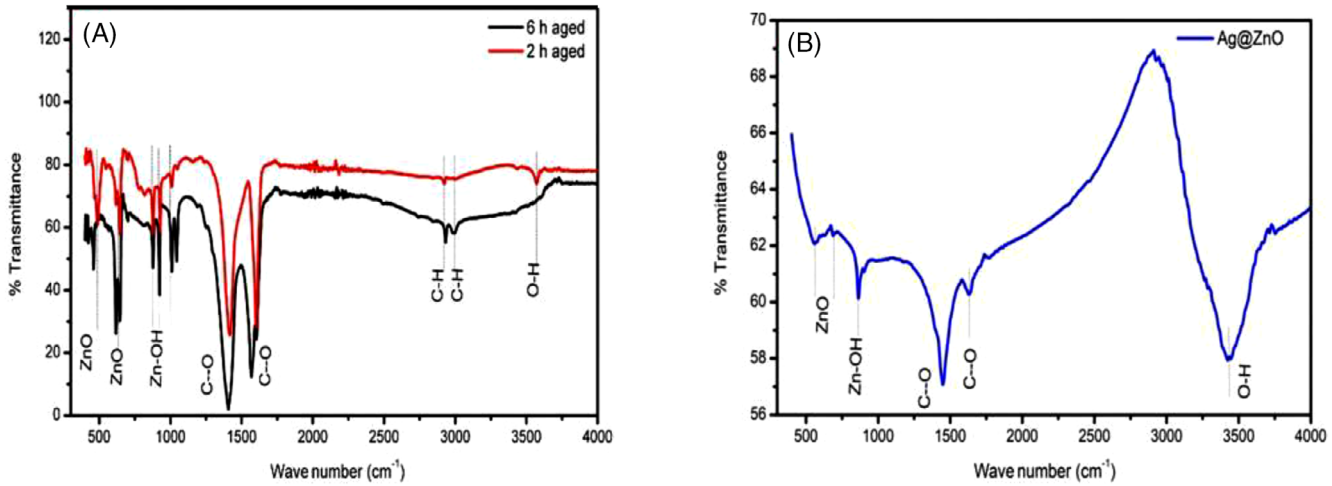

FIGURE 8 Fourier transform infrared (FTIR) spectra of samples after (A) 6 and 2 h aging times and (B) Ag@ZnO.

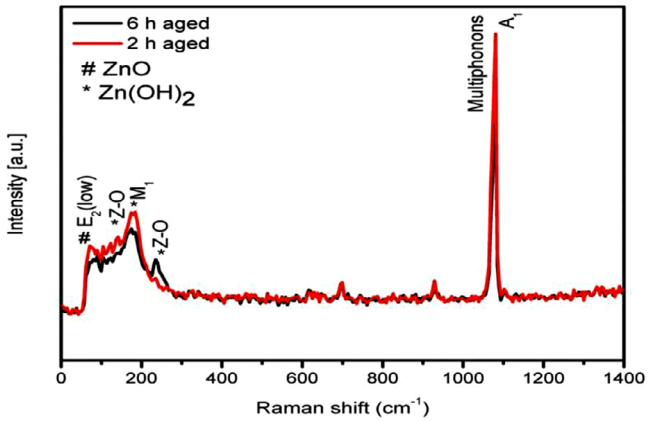

FIGURE 9 Raman spectra of the $Zn(OH)_2$ and ZnO after 6 and 2 h aging times.

The Raman spectrum (Figure 9) showed the peaks of vibration modes from ZnO and $Zn(OH)_2$. The peak with the maximum intensity of 99 cm^{-1} corresponded to the (low) vibration mode E_2. Additionally, multiphonons with A_1 symmetry can be observed at 1075 cm^{-1}. The peaks below 350 cm^{-1} correspond to lower corresponded to high-energy vibration modes.[39] The maximum intensities found at 142 and 234 cm^{-1} were attributed to ZnO translational vibration modes. Other vibration combinations (M_1) were found at 178 cm^{-1}.[40] Therefore, the Raman spectrum supports the experimental data obtained from XRD and FTIR, a material containing a mixture of ZnO and $Zn(OH)_2$.

3.6 | Photocatalytic investigations

The photocatalytic performance of the samples synthesized in the framework of this study has also been investigated. In the experimental setting, UVA light was employed as the irradiation source, whereas RhB was used as the dyestuff. As the energy of the UVA light is relatively close to the visible region, the degradation of the RhB dye can be easily observed by optical absorption spectroscopy. Therefore, in many cases, UVA radiation interacts with molecules and materials similarly to visible light, and it has sufficient energy to initiate chemical changes in RhB dye molecules.

Faheem et al.[28] concluded that the $ZnO/Zn(OH)_2$ structure adsorbs more dyestuff than pure ZnO, thanks to the presence of surface hydroxyl (–OH) groups that can develop non-covalent interactions with the dye molecule. As a result of this structural formation, photocatalytic processes are promoted by the increased adsorption of dye molecules, and the performance of the photocatalyst increases. We synthesized the $ZnO/Zn(OH)_2$ structure instead of pure ZnO. The surface features of the catalysts also play an essential role in the charge–transfer process of dyestuffs such as RhB and photo-degradation, which is responsible for dye adsorption. The formation of reactive oxygen species (ROS), which is one of the important parameters in photo-catalysis applications where ZnO is used as catalyst and RhB as dyestuff, is described in detail in Ref. [41]. Figure 10A shows that each catalyst stably degraded the RhB dye. According to the findings of a newly published publication by our research group,[42] the negative charge repulsion between the catalyst surface and the dyestuff might slow down the degradation process. As a result, the slow decline curve seen in Figure 10B for RhB can be attributed to this.

Moreover, the photo-degradation of the RhB dyestuff on $ZnO/Zn(OH)_2$ was observed to be 98.5% and 92.5% for 6 and 2 h aged samples, respectively, after 180 min. In order to increase the photocatalytic activity of the sample subjected

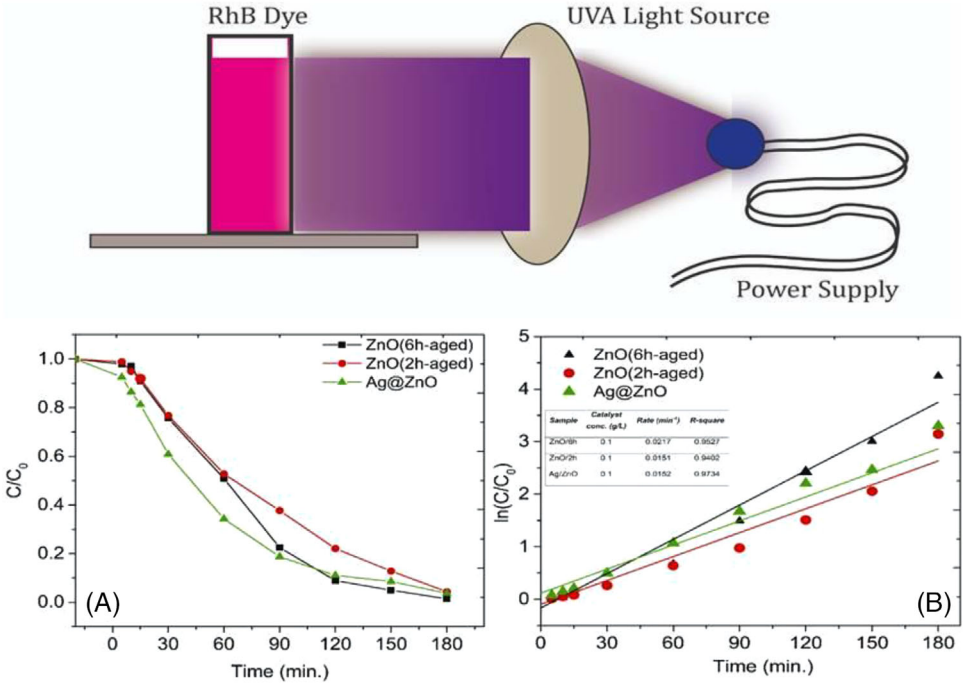

FIGURE 10 Experimental setup used for photocatalytic measurement (*), time depended on C/C_0 curves (A) and pseudo-first-order kinetics of the photocatalytic degradation (B).

to a 2 h drying process, Ag NPs were decorated to the sample surface as seen in SEM photographs (Figure 6C), and the catalytic performance of the sample was increased up to 95%. The Ag NPs' SPR properties allow for greater light absorption, particularly in the UV and visible range. This is advantageous compared to pure $ZnO/Zn(OH)_2$ material due to its wider band gap. This broadening of the absorption range leads to the formation of more electron–hole pairs, which is essential for efficient photo-catalysis. In addition, Ag NPs contribute additional charge carriers to the composite system through SPR-mediated electron excitation. When Ag NPs absorb photons and generate hot electrons, these electrons can be effectively injected into the conduction band of $ZnO/Zn(OH)_2$. This procedure enhances the quantity of charge carriers accessible for catalytic reactions, subsequently promoting photocatalytic activity. The salient aspect is the lessening of electron–hole recombination, as it is fundamental for achieving effective photo-catalysis. This occurrence prolongs the lifespan of charge carriers in the composite system and lessens the likelihood of recombination. The prolonged recombination time enables more charge carriers to take part in redox reactions on the surface of $ZnO/Zn(OH)_2$, thereby boosting photocatalytic efficacy. According to the literature,[43–46] numerous parameters, such as the surface morphology of the catalyst and the optical band gap, have a direct impact on the catalyst's performance in photocatalytic applications.

Meanwhile, Uma et al.[47] demonstrated that the optical band gap of ZnO reduced in the composite ZnO film formed by using gC_3N_4, making ZnO highly performant in the photocatalytic degradation of RhB dyestuff. Moreover, efficient photocatalytic degradation may result from the high concentration of defects on the surfaces of ZnO nanostructures and hence from surface morphology.[48] From this, the observed decrease in the optical band gap of $ZnO/Zn(OH)_2$ NPs after Ag decoration may be closely linked to the enhanced photocatalytic performance. Ag NPs' SPR properties increase the formation of charge carriers by capturing and transferring incident light energy. This effect, combined with their ability to minimize electron–hole recombination, contributes to the superior photocatalytic effectiveness observed in the scope of this investigation. Moreover, taking all these considerations into account, the low optical band gap and particle size, as well as the rod-like morphology, explain why the sample obtained by 6 h aging is relatively more efficient in removing RhB dye.

Table 2 compares the performance of ZnO catalysts recently synthesized with different characteristics and used in the photocatalytic decomposition of RhB dye. According to this, it is seen that RhB dyestuff is degraded between 60% and 98% depending on different UV or sunlight irradiation times. Therefore, the easily synthesized $ZnO/Zn(OH)_2$ catalyst proposed in this study is more

TABLE 2 Performance of ZnO catalysts with different characteristics in photocatalytic degradation of rhodamine B (RhB) dye.

Catalyst	Pollutant	% Degradation	Time interval (min)	Refs.
Al/ZnO	RhB	97	120	[49]
ZnO nano-disc	RhB	90	90	[50]
ZnO nanostructure	RhB	97.75	70	[51]
ZnO nano-powder	RhB	>95	80	[52]
ZnO film	RhB			[11]
Ba/ZnO	RhB	88.81	160	[54]
ZnO nanoparticles	RhB	95.41	160	[55]
B/Sn-doped ZnO nanoparticles	RhB	65.6	60	[56]
ZnO nanoparticles	RhB	>95	120	[57]
ZnO nanopowder	RhB	98.5	180	This work

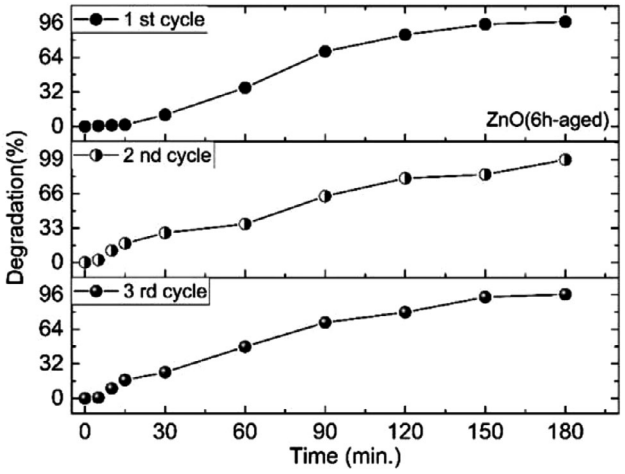

FIGURE 11 Photo-stability test of $ZnO/Zn(OH)_2$ during RhB degradation.

performant than the literature in Table 2 for the degradation of RhB dye and may be preferable and improved for the researchers. Besides, the degradation costs of dyes and toxic molecules are another important parameter for photo-catalysis applications. Therefore, it is very important to investigate the reusability of photocatalyst materials. At this point, it is expected that the corrosion that may occur in ZnO during the photo-catalysis process will not impair the photo-stability of ZnO. The photo-degradation of RhB by $ZnO/Zn(OH)_2$ (aged for 6 h) was carried out for three repeated cycles to observe whether this occurs.

According to Figure 11, $ZnO/Zn(OH)_2$ NPs exhibited good photostability, supporting their reusability after each cycle. Nevertheless, a slight decrease in performance was observed in cycle 3. The possibility of dissolution of ZnO by photo-corrosion was considered a possible reason for this slight decrease in degradation efficiency. When the time-dependent C/C_0 data given in Figure 10A are plotted in terms of $\ln(C_o/C)$, linear graphs are obtained, showing that the degradation follows first-order kinetics independent of the morphology of the ZnO particles. Langmuir–Hinshelwood kinetic equations are often used to describe first-order degradation.[58,59] The pseudo-first-order rate constants (k) and R-square values obtained according to this approach have been tabulated in Figure 10B. As can be seen from this table, the highest k value for RhB dye for 0.0217 was obtained for the ZnO catalyst aged for 6 h. Furthermore, the correlation coefficient values R for all catalysts were calculated around .95, confirming the proposed kinetic model for the de-colorization of RhB dyes.

4 | CONCLUSION

$ZnO/Zn(OH)_2$ composite NPs were prepared by the sol–gel method using solutions aged at different times in the spin coating device. Among these samples, it was seen that the sample with the solution aged for 6 h was found to have the best structural and optical properties. XRD diffraction patterns showed that ZnO NPs, Ag NPs, and Ag@ZnO core–shell nanostructures were polycrystalline. UV–vis spectrometry results confirmed that the decrease in the band gap of both ZnO and $Zn(OH)_2$ phases was observed with the addition of Ag NPs on the surface of the $ZnO/Zn(OH)_2$ structure. SEM images revealed that ZnO and Ag NPs were found and were seen as bright particles. The characteristic elements Zn, O, and C were determined in the elemental analysis of the samples obtained after 6 and 2 h of aging. In addition, the RhB dye removal from aqueous solutions with Ag-decorated ZnO nanostructure was investigated. The results obtained from the study show us that it is an adsorbent that can be used efficiently in removing Ag@ZnO by the adsorption method. In addition, reusability tests were carried out using the best catalyst $ZnO/Zn(OH)_2$ (aged for 6 h). It was found that the degradation percentages were higher in the third cycle. The highest

pseudo-first-order rate constant (k) and R-square values for RhB dye were found to be 0.0217 and 0.95, respectively.

ACKNOWLEDGMENTS

None.

ORCID

Erman Erdogan https://orcid.org/0000-0003-2566-3284
Mehmet Yilmaz https://orcid.org/0000-0002-4368-8453

REFERENCES

1. Pathakoti K, Manubolu M, Hwang HM. Nanotechnology applications for environmental industry. In: Handbook of nanomaterials for industrial applications. Amsterdam: Elsevier; 2018. p. 894–907.
2. Chavali MS, Nikolova MP. Metal oxide nanoparticles and their applications in nanotechnology. SN Appl Sci. 2019;1(6):607.
3. Hassan JJ, Mahdi MA, Chin CW, Abu-Hassan H, Hassan Z. A high-sensitivity room-temperature hydrogen gas sensor based on oblique and vertical ZnO nanorod arrays. Sens Actuators, B: Chem. 2013;176:360–67.
4. Kumawat A, Misra KP, Chattopadhyay S. Band gap engineering and relationship with luminescence in rare-earth elements doped ZnO: an overview. Mater Technol. 2022;37(11):1595–610.
5. Hassan JJ, Mahdi MA, Yusof Y, Abu-Hassan H, Hassan Z, Al-Attar HA, et al. Fabrication of ZnO nanorod/p-GaN high-brightness UV LED by microwave-assisted chemical bath deposition with $Zn(OH)_2$–PVA nanocomposites as seed layer. Opt Mater. 2013;35(5):1035–41.
6. Colak H, Mercan HI. Influence of thallium doping on structural, electrical, and optical properties of ZnO nanorods for TCO applications. J Mater Sci: Mater Electron. 2022;33(18):14816–28.
7. Samad A, Furukawa M, Katsumata H, Suzuki T, Kaneco S. Photocatalytic oxidation and simultaneous removal of arsenite with CuO/ZnO photocatalyst. J Photochem Photobiol, A. 2016;325:97–103.
8. Hanh NT, Tri NLM, Van Thuan D, Tung MHT, Pham TD, Minh TD, et al. Monocrotophos pesticide effectively removed by novel visible light driven Cu doped ZnO photocatalyst. J Photochem Photobiol, A. 2019;382:111923.
9. Isai KA, Shrivastava VS. Photocatalytic degradation of methylene blue using ZnO and 2% Fe–ZnO semiconductor nanomaterials synthesized by sol–gel method: a comparative study. SN Appl Sci. 2019;1:1–11.
10. Farhad SFU, Tanvir NI, Bashar MS, Sultana M. Synthesis and characterization of c-axis oriented zinc oxide thin film and its use for the subsequent hydrothermal growth of zinc oxide nanorods. MRS Adv. 2019;4(16):921–28.
11. Mahajan P, Datt R, Gupta V, Arya S. Synthesis and characterization of ZnO@ WO_3 core/shell nanoparticles as counter electrode for dye-sensitized solar cell. Surf Interfaces. 2022;30:101920.
12. Ghos BC, Farhad SFU, Patwary MAM, Majumder S, Hossain MA, Tanvir NI, et al. Influence of the substrate, process conditions, and postannealing temperature on the properties of ZnO thin films grown by the successive ionic layer adsorption and reaction method, ACS Omega. 2021;6:2665–74.
13. Ben Aziza M, Litaiem Y, Chtourou R, Ammar S. The influence of different stabilizers on properties of sol–gel spin-coated zinc oxide films. Braz J Phys. 2021;51:722–30.
14. Arya S, Mahajan P, Mahajan S, Khosla A, Datt R, Gupta V, et al. Influence of processing parameters to control morphology and optical properties of sol-gel synthesized ZnO nanoparticles. ECS J Solid State Sci Technol. 2021;10(2):023002.
15. He X, Yang Y, Li Y, Chen J, Yang S, Liu R, et al. Effects of structure and surface properties on the performance of ZnO towards photocatalytic degradation of methylene blue. Appl Surf Sci. 2022;599:153898.
16. Zhang Q, Xu M, You B, Zhang Q, Yuan H, Ostrikov K. Oxygen vacancy-mediated ZnO nanoparticle photocatalyst for degradation of methylene blue. Appl Sci. 2018;8(3):353.
17. Ahumada-Lazo R, Torres-Martínez LM, Ruíz-Gómez MA, Vega-Becerra OE, Figueroa-Torres MZ. Photocatalytic efficiency of reusable ZnO thin films deposited by sputtering technique. Appl Surf Sci. 2014;322:35–40.
18. Sheikhi S, Aliannezhadi M, Tehrani FS. Effect of precursor material, pH, and aging on ZnO nanoparticles synthesized by one-step sol–gel method for photodynamic and photocatalytic applications. Eur Phys J Plus. 2022;137(1):60.
19. Taşyürek LB, Aydoğan Ş, Sevim M, Çaldıran Z. Synthesis of nickel nanoparticles-deposited strontium titanate nanocubes (Ni-STO) and heterojunction electrical applications over a wide temperature range. Mater Sci Eng: B. 2021;274:115479.
20. El Hallani G, Fazouan N, Liba A, Khuili M. The effect of sol aging time on structural and optical properties of sol–gel ZnO doped Al. J Phys Conf Ser. 2016;758(1):012021.
21. Zhang S, Lu H, Rui G, Lv C, He J, Cui Y, et al. Preparation of Ag@ ZnO core–shell nanostructures by liquid-phase laser ablation and investigation of their femtosecond nonlinear optical properties. Appl Phys B. 2020;126:1–9.
22. Sakir M, Salem S, Sanduvac ST, Sahmetlioglu E, Sarp G, Onses MS, et al. Photocatalytic green fabrication of Au nanoparticles on ZnO nanorods modified membrane as flexible and photocatalytic active reusable SERS substrates. Colloids Surf A. 2020;585:124088.
23. Erdoğan E, Turgut G, Yilmaz M. Sol–gel spin coating derived cadmium oxide semiconductor thin films: effect of lutetium contribution. Optik. 2021;240:166819.
24. Erdoğan E, Yilmaz M, Aydogan S, Turgut G. Investigation of neodymium rare earth element doping in spray-coated zinc oxide thin films. J Mater Sci: Mater Electron. 2021;32:1379–91.
25. Devesa S, Rooney AP, Graça MP, Cooper D, Costa LC. Williamson-hall analysis in estimation of crystallite size and lattice strain in $Bi_{1.34}Fe_{0.66}Nb_{1.34}O_{6.35}$ prepared by the sol–gel method. Mater Sci Eng: B. 2021;263:114830.
26. Escobedo-Morales A, Ruiz-López II, Ruiz-Peralta MD, Tepech-Carrillo L, Sánchez-Cantú M, Moreno-Orea JE. Automated method for the determination of the band gap energy of pure and mixed powder samples using diffuse reflectance spectroscopy. Heliyon. 2019;5(4):e01505.
27. Ahmed DS, Al-Baidhani M, Adil H, Bufaroosha M, Rashad AA, Zainulabdeen K, et al. Recent study of PF/ZnO nanocomposites: synthesis, characterization and optical properties. Mater Sci Energy Technol. 2023;6:29–34.

28. Faheem M, Siddiqi HM, Habib A, Shahid M, Afzal A. $ZnO/Zn(OH)_2$ nanoparticles and self-cleaning coatings for the photocatalytic degradation of organic pollutants. Front Environ Sci. 2022;10:1159.
29. Hassan JJ, Mahdi MA, Chin CW, Hassan Z, Abu-Hassan H. Microwave-assisted chemical bath deposition of vertically aligned ZnO nanorods on a variety of substrates seeded by PVA–$Zn(OH)_2$ nanocomposites. Appl Surf Sci. 2012;258(10): 4467–72.
30. Vinh THT, Thuy NTB, Thi CM, Van Viet P. Visible-light-driven photo-catalysis of anisotropic silver nanoparticles decorated on ZnO nanorods: synthesis and characterizations. J Environ Chem Eng. 2021;9(2):105103.
31. Mosquera E, Rojas-Michea C, Morel M, Gracia F, Fuenzalida V, Zárate RA. Zinc oxide nanoparticles with incorporated silver: structural, morphological, optical and vibrational properties. Appl Surf Sci. 2015;347:561–68.
32. El-Bindary AA, El-Marsafy SM, El-Maddah AA. Enhancement of the photocatalytic activity of ZnO nanoparticles by silver doping for the degradation of AY99 contaminants. J Mol Struct. 2019;1191:76–84.
33. Kumar RRC, Betageri VS, Nagaraju G, Pujar GH, Onkarappa HS, Latha MS. Synthesis of core/shell (ZnO/Ag) nanoparticles using *Calotropis gigantea* and their applications in photocatalytic and antibacterial studies. J Inorg Organomet Polym Mater. 2020;30(9):3410–17.
34. Top A, Çetinkaya H. Zinc oxide and zinc hydroxide formation via aqueous precipitation: effect of the preparation route and lysozyme addition. Mater Chem Phys. 2015;167:77–87.
35. Balogun SW, James OO, Sanusi YK, Olayinka OH. Green synthesis and characterization of zinc oxide nanoparticles using bashful (*Mimosa pudica*), leaf extract: a precursor for organic electronics applications. SN Appl Sci. 2020;2:1–8.
36. Sagadevan S, Pal K, Chowdhury ZZ, Hoque ME. Structural, dielectric and optical investigation of chemically synthesized Ag-doped ZnO nanoparticles composites. J Sol–Gel Sci Technol. 2017;83:394–404.
37. da Silva-Neto ML, de Oliveira MC, Dominguez CT, Lins RE, Rakov N, de Araújo CB, et al. UV random laser emission from flexible ZnO-Ag-enriched electrospun cellulose acetate fiber matrix. Sci Rep. 2019;9(1):1–9.
38. Tran TT, Vu XH, Ngo TL, Pham TTH, Nguyen DD. Enhanced Raman scattering based on a ZnO/Ag nano-structured substrate: an in-depth study of the SERS mechanism. Phys Chem Chem Phys. 2023;25(23):15941–52.
39. Gordeeva A, Hsu YJ, Jenei IZ, Brant Carvalho PH, Simak SI, Andersson O, et al. Layered zinc hydroxide dihydrate, $Zn_5(OH)_{10}\cdot 2H_2O$, from hydrothermal conversion of ε-$Zn(OH)_2$ at gigapascal pressures and its transformation to nanocrystalline ZnO. ACS Omega. 2020;5(28):17617–27.
40. Varella Rodrigues A, Domingos Onishi BS, Ribeiro SJL. Facile formation of sulfurized nanorod-like $ZnO/Zn(OH)_2$ and hierarchical flower-like γ-$Zn(OH)_2$/ε-$Zn(OH)_2$ from a green synthesis and application as luminescent solar concentrator. ChemPhysChem. 2023;24:e202300134.
41. Piva DH, Piva RH, Rocha MC, Dias JA, Montedo ORK, Malavazi I, et al. Antibacterial and photocatalytic activity of ZnO nanoparticles from $Zn(OH)_2$ dehydrated by azeotropic distillation, freeze drying, and ethanol washing. Adv Powder Technol. 2017;28(2):463–72.
42. Davaslıoğlu İÇ, Özdokur KV, Koçak S, Çırak Ç, Çağlar B, Çırak BB, et al. WO3 decorated TiO2 nanotube array electrode: preparation, characterization and superior photoelectrochemical performance for rhodamine B dye degradation. J Mol Struct. 2021;1241:130673.
43. Le Bahers T, Rerat M, Sautet P. Semiconductors used in photovoltaic and photocatalytic devices: assessing fundamental properties from DFT. J Phys Chem C. 2014;118(12): 5997–6008.
44. Kadhim MJ, Mahdi MA, Selman AM, Al-Ani JSK, Hassan JJ, Ahmed NM. The most important parameters that affect the photocatalytic activity of ZnO nanostructures against organic dyes: a review. Iran J Catal. 2023;13(1):1–21.
45. Kadhim MJ, Mahdi MA, Hassan JJ. Influence of pH on the photocatalytic activity of ZnO nanorods. Mater Int. 2020;2:0064–0072.
46. Kadhim MJ, Allawi F, Mahdi MA, Najah Abaas S. High photocatalytic performance in the photo-degradation of MB Dye of photocatalytic efficiency of ZnO/Fe_3O_4 and TiO_2/Fe_3O_4 under visible light irradiation. Iran J Mater Sci Eng. 2022;19(3):16–23.
47. Uma R, Ravichandran K, Sriram S, Sakthivel B. Cost-effective fabrication of $ZnO/g\text{-}C_3N_4$ composite thin films for enhanced photocatalytic activity against three different dyes (MB, MG and RhB). Mater Chem Phys. 2017;201:147–55.
48. Rahman QI, Ahmad M, Misra SK, Lohani MB. Hexagonal ZnO nanorods assembled flowers for photocatalytic dye degradation: growth, structural and optical properties. Superlattices Microstruct. 2013;64:495–506.
49. Trang TNQ, Phan TB, Nam ND, Thu VTH. In situ charge transfer at the Ag@ ZnO photoelectrochemical interface toward the high photocatalytic performance of H2 evolution and RhB degradation. ACS Appl Mater Interfaces. 2020;12(10):12195–206.
50. Seo HK, Shin HS. Study on photocatalytic activity of ZnO nanodisks for the degradation of rhodamine B dye. Mater Lett. 2015;159:265–68.
51. Nandi P, Das D. Photocatalytic degradation of rhodamine-B dye by stable ZnO nanostructures with different calcination temperature induced defects. Appl Surf Sci. 2019;465:546–56.
52. Nagaraja BK, Tripathy R, Ramchand CN, Sundararaman M. Bioautography guided identification of anticandidal compounds from A. terreus st. 1. Am J Infect Dis. 2011;7(4):91.
53. Boughelout A, Macaluso R, Kechouane M, Trari M. Photocatalysis of rhodamine B and methyl orange degradation under solar light on ZnO and Cu_2O thin films. React Kinet Mech Catal. 2020;129:1115–30.
54. Shirdel B, Behnajady MA. Visible-light-induced degradation of rhodamine B by Ba doped ZnO nanoparticles. J Mol Liq. 2020;315:113633.
55. Dodoo-Arhin D, Asiedu T, Agyei-Tuffour B, Nyankson E, Obada D, Mwabora JM. Photocatalytic degradation of rhodamine dyes using zinc oxide nanoparticles. Mater Today: Proc. 2021;38:809–15.
56. Ahmed AZ, Islam MM, Islam MMU, Masum SM, Islam R, Molla MAI. Fabrication and characterization of B/Sn-doped ZnO nanoparticles via mechanochemical method for photocat-

alytic degradation of rhodamine B. Inorg Nano-Metal Chem. 2020;51(10):1369–78.

57. Ali MA, Idris MR, Quayum ME. Fabrication of ZnO nanoparticles by solution-combustion method for the photocatalytic degradation of organic dye. J Nanostruct Chem. 2013;3:1–6.
58. Ong CB, Ng LY, Mohammad AW. A review of ZnO nanoparticles as solar photocatalysts: synthesis, mechanisms and applications. Renew Sustain Energy Rev. 2018;81:536–51.
59. Zheng X, Zhang D, Gao Y, Wu Y, Liu Q, Zhu X. Synthesis and characterization of cubic Ag/TiO_2 nanocomposites for the photocatalytic degradation of methyl orange in aqueous solutions. Inorg Chem Commun. 2019;110:107589.

How to cite this article: Erdogan E, Eden C, Canpolat N, Cirak C, Yilmaz M. Optimizing the structural and photocatalytic performance of Ag-decorated ZnO/$Zn(OH)_2$ nanoparticles for RhB degradation. Int J Appl Ceram Technol. 2024;21:2010–23. https://doi.org/10.1111/ijac.14675